

# Discovery of K-shell Emission Lines of Neutral Atoms in the Galactic Center Region

Masayoshi NOBUKAWA<sup>1</sup>, Katsuji KOYAMA<sup>1</sup>, Takeshi Go TSURU<sup>1</sup>, Syukyo G RYU<sup>1</sup>, and Vincent TATISCHEFF<sup>2</sup>

<sup>1</sup>*Department of Physics, Graduate school of Science, Kyoto University, Sakyo-ku, Kyoto 606-8502*

*nobukawa@cr.scphys.kyoto-u.ac.jp*

<sup>2</sup>*Centre de Spectrométrie Nucléaire et de Spectrométrie de Masse, IN2P3-CNRS and Univ Paris-Sud, 91405, Orsay, France*

(Received ; accepted )

## Abstract

The K-shell emission line of neutral irons from the Galactic center (GC) region is one of the key for the structure and activity of the GC. The origin is still open question, but possibly due either to X-ray radiation or to electron bombarding to neutral atoms. To address this issue, we analyzed the Suzaku X-ray spectrum from the GC region of intense neutral iron line emission, and report on the discovery of  $K\alpha$  lines of neutral argon, calcium, chrome, and manganese atoms. The equivalent widths of these  $K\alpha$  lines indicate that the metal abundances in the GC region should be  $\sim 1.6$  and  $\sim 4$  of solar value, depending on the X-ray and the electron origins, respectively. On the other hand, the metal abundances in the hot plasma in the GC region are found to be  $\sim 1$ – $2$  solar. These results favor that the origin of the neutral  $K\alpha$  lines are due to X-ray irradiation.

**Key words:** Galaxy: center — X-rays: ISM — ISM: clouds — ISM: abundances

## 1. Introduction

ASCA found clumpy structures of the 6.4 keV line in the Sagittarius (Sgr) B2 and the Radio Arc regions (Koyama et al. 1996). Since the clumps correspond to giant molecular clouds, we refer to them as a "neutral clump" hereafter.

The X-ray spectrum of the Sgr B2 neutral clump has a prominent 6.4 keV line on the continuum emission with deep absorption of  $N_{\text{H}} \sim 10^{24} \text{ cm}^{-2}$  (Murakami et al. 2000). Recently, many new neutral clumps M0.74–0.09, M0.51–0.10 (Sgr B1), G0.174–0.233, M359.47–0.15, M359.43–0.07, M359.43–0.12, M359.38–0.00 have been discovered (Koyama et al. 2007c; Yusef-Zadeh et al. 2007; Nobukawa et al. 2008; Fukuoka et al. 2009; Nakajima et al. 2009).

The origin of a neutral clump, particularly the 6.4 keV line, is one of the open questions among high energy phenomena in the Galactic center (GC) region. Koyama et al. (1996) and Murakami et al. (2000) suggested that the 6.4 keV emission from the neutral clumps is due to the K-shell ionization of iron atoms by external X-rays, possibly from the super-massive black hole, Sgr A\* (an X-ray reflection nebula; XRN). Although the present X-ray luminosity of Sgr A\* is  $\sim 10^{33-35} \text{ erg s}^{-1} \text{ cm}^{-2}$  (Baganoff et al. 2001, 2003), the luminosity required for the 6.4 keV emission is  $10^{38-39} \text{ erg s}^{-1} \text{ cm}^{-2}$ . Therefore, Sgr A\* in a few hundred years ago would have been  $10^{3-6}$  times brighter than now (e. g. Koyama et al. 1996). On the other hand, Yusef-Zadeh et al. (2007) proposed that the origin of the 6.4 keV emission would be low energy cosmic-ray electrons ( $E_e = 10$ – $100 \text{ keV}$ ), because they found that the X-rays correlated with non-thermal radio filaments.

Neutral atoms of lighter elements, such as Ar and Ca,

should also exist in the neutral clumps, and hence would emit K-shell emission lines. These would provide new information to constrain the origin of the neutral clumps in the GC region. However only the K-shell lines of neutral Fe and Ni atoms have been discovered so far (but see Fukuoka et al. 2009).

The Sgr A region is the best place for the search of neutral K-shell lines of various elements because many bright neutral clumps have been found at  $(l, b) \sim (0^\circ 1, -0^\circ 1)$  (Tsuboi et al. 1999) and many observations have been performed with Suzaku (Koyama et al. 2007b; Hyodo et al. 2009).

We re-analyzed the X-ray data obtained with the X-ray Imaging Spectrometers (XIS; Koyama et al. 2007a) aboard Suzaku (Mitsuda et al. 2007) and found emission lines from neutral Ar, Ca, Cr, and Mn atoms. This paper reports on a detailed analysis, results, and discussion on the origin.

## 2. Observations and Data Reduction

The eastern vicinity of Sgr A\* was observed 4 times in 2005, 2006, and 2007 with Suzaku. Each pointing angle was almost the same. The observation information is listed in table 1.

The XIS consist of three front-illuminated (FI; XIS0, 2, and 3) and one back-illuminated (BI; XIS1) CCD camera systems. All of the XIS are placed on the focal planes of the X-Ray Telescopes (XRT; Serlemitsos et al. 2007). The size of the field of view is  $17'8 \times 17'8$  and the half-power diameter is  $1'9$ – $2'3$ . XIS2 has been out of use since 2006 November, hence we did not use the XIS2 data on the 2007 September.

The XIS was working with the normal clocking and the

**Table 1.** Observation Data List.

Observation ID	R.A.	Decl.	XIS	SCI	obs start	exposure time*
100027010	266.5146	-28.9267	0 1 2 3	off	2005-09-23	44.8 ks
100037040	266.5133	-28.9266	0 1 2 3	off	2005-09-30	43.0 ks
100048010	266.5135	-28.9269	0 1 2 3	off	2006-09-08	63.0 ks
102013010	266.5129	-28.9278	0 1 3	on	2007-09-03	51.4 ks

\*After the data screening described in the text.

full-window mode during all observations. The XIS pulse-height data for each X-ray event were converted to Pulse Invariant (PI) channels using the `xispi` software version 2008-04-10, and the calibration database version 2008-08-25. We removed the data during the epoch of low-Earth elevation angles of less than  $5^\circ$  ( $\text{ELV} < 5^\circ$ ), day Earth elevation angles of less than  $10^\circ$  ( $\text{DYE\_ELV} < 10^\circ$ ), and the South Atlantic Anomaly. The good exposure times are listed in table 1.

Since the XIS CCDs have been gradually degraded by on-orbit particle radiation, the CCD performances have been restored by the Spaced-row charge injection (SCI) technique since 2006 October (Uchiyama et al. 2009). Thus, the data in 2007 September were taken with the SCI technique. The overall spectral resolutions (FI/BI) at 5.9 keV were 150/150, 175/185, and 140/175 eV (FWHM) for the 2005, 2006, and 2007 observations, respectively.

Since the non-X-ray background (NXB) depends on the geomagnetic cut-off rigidity (COR) (Tawa et al. 2008), we sorted the NXB with the COR values, using `xisnxbgen`, from the night-Earth data released by the Suzaku XIS team. The COR-sorted NXB was subtracted from the raw data with the same COR.

Since the relative gain of the FI sensors were well calibrated and the response functions were essentially the same, we co-added the FI data. We also summed the spectra of the four observations to increase the statistics.

We analyzed the data using the software package HEASoft 6.6.1. For spectral fittings, we made XIS response files using `xismfgen`, and auxiliary files using `xissimarfgen`.

### 3. Analysis and Results

#### 3.1. 6.4 keV line Image

In order to depict a neutral clump from the GC region, we made an X-ray image in the 6.4 keV line by the following procedures. We first made X-ray images in the 5–6 keV and in the 6.3–6.5 keV bands, after subtracting the NXB and correcting the vignetting effect. We extracted the X-ray spectrum from a  $8'$  circular region near the field center, and fitted the 5–6 keV band spectrum with a power-law model. The best-fit photon index in the 5.0–6.0 keV band is  $1.25 \pm 0.07$ . The ratio of the photon flux in the 6.3–6.5 keV band to that in the 5.0–6.0 keV band was estimated to be 0.165, by extrapolation of the power-law index. We multiplied the 5.0–6.0 keV band image by 0.165, and subtracted from the 6.3–6.5 keV band image. The result is shown in figure 1.

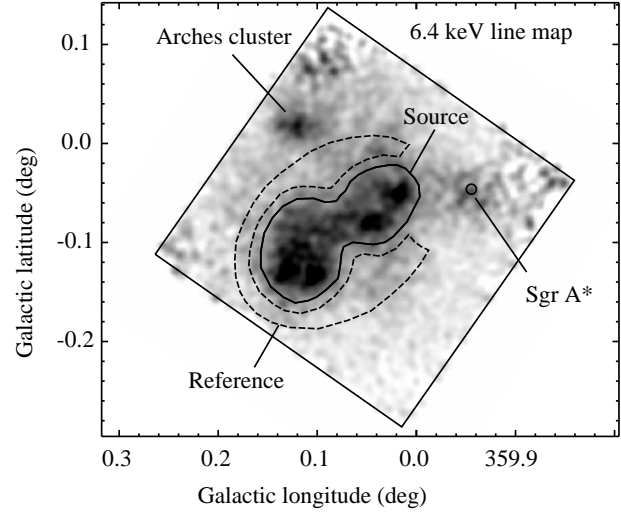


**Fig. 1.** X-ray image in the 6.4 keV neutral iron line (the underlying continuum fluxes are subtracted). The solid square is the field of view (FOV) of the XIS. The small circle indicates the position of Sgr A\*. We extracted the source spectrum from the solid region (Source). In order to examine the contribution of the GC hot plasma, we also selected the surrounding region (Reference) marked with the dashed line. The areas of the Source and Reference regions are 43.3 and 40.5 arcmin<sup>2</sup>, respectively. The bright source in the northeast edge of the FOV is the Arches cluster (e.g., Tsujimoto et al. 2007).

We can see a bright region near the center of the 6.4 keV line image, as is shown with the solid line of a gourd-like shape (hereafter, the Source region). Around the Source region, we can see fainter emissions, which may be due to unresolved minor neutral clumps.

The X-ray emission from the GC hot plasma contributes to the spectrum of the Source region. In order to examine the contribution of the GC hot plasma accurately, we selected the dashed region, excluding the supernova remnant, Sgr A East (Maeda et al. 2002), whose size and position are  $\sim 3'$  and  $(l, b) \sim (-359^\circ 5, -0^\circ 5)$ . Hereafter, we call this region as Reference.

#### 3.2. Gain Tuning

The nominal uncertainty of the absolute energy of XIS is  $\sim 10$  eV (the Suzaku XIS team<sup>1</sup>). To be more accurate, we checked the energy of the  $K\alpha$  lines of H-like S (S XV)

<sup>1</sup> [http://www.astro.isas.ac.jp/suzaku/doc/suzaku\\_td](http://www.astro.isas.ac.jp/suzaku/doc/suzaku_td)

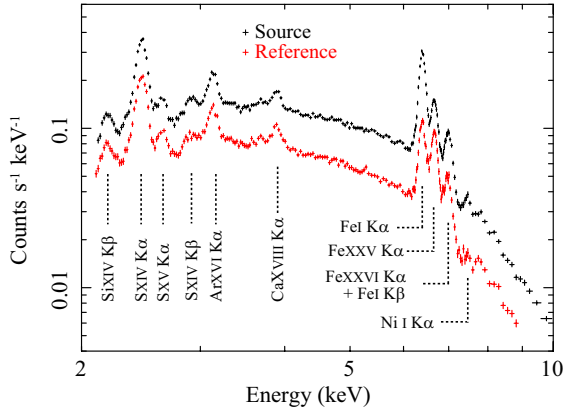


**Fig. 2.** X-ray Spectra (FI) in the Source (black) and the Reference (red) regions, where the NXB was already subtracted. Identified emission lines are indicated by the dashed lines with their corresponding elements. Errors of the data are estimated at the  $1\sigma$  confidence level.

of the spectra and the calibration source  $^{55}\text{Fe}$  (emits the  $\text{Mn I K}\alpha$  line at 5895 eV) attached at the corner of the XIS. Compared with the theoretical value obtained from Atomic & Molecular Database in the Institute of Applied Physics and Computational Mathematics (CAMDB)<sup>2</sup>, we found that the energy differences of  $\text{S XV K}\alpha$  and  $\text{Mn I K}\alpha$  were  $5 \pm 2$  and  $0 \pm 1$  eV for FI, while those for BI were consistent with the theoretical energies. We, therefore, fine-tuned the energy scale for FI as a liner function;

$$\Delta E = -0.0015 \times (E_0 - 5895) \text{ (eV)}, \quad (1)$$

where  $E_0$  and  $\Delta E$  are the original and energy shift, respectively.

### 3.3. Model Construction

Figure 2 shows the X-ray spectra of the FI sensor in the Source and Reference regions. The spectra have several ionized emission lines of heavy elements, such as Si, S, Ar, Ca, and Fe. These lines would come from the GC hot plasma with the temperature of  $kT \sim 7$  keV (Koyama et al. 2007b) and possibly  $kT \sim 1$  keV (Ryu et al. 2009).

On the other hand, we can see prominent  $\text{K}\alpha$  lines of neutral Fe and Ni at 6.4 keV and 7.5 keV in the spectra. The neutral lines indicate the existence of a large amount of neutral Fe and Ni atoms in the regions. The neutral lines from the Reference region may be due to many faint unresolved neutral clumps.

The X-ray spectra of the two regions (Source and Reference) would be a complex of the GC hot plasma and the neutral clumps (Koyama et al. 2009; Ryu et al. 2009). We, therefore, made a fitting model composed of the GC hot plasma (here *Plasma*), the neutral clumps (here *Neutral*) and the Cosmic X-ray background (here *CXB*). Thus, the model is given by;

$$\text{Model} = \text{Abs1} \times [\text{Plasma} + \text{Neutral}] + \text{CXB}, \quad (2)$$

where *Abs1* is absorption of the inter-stellar medium to-

ward the GC region.

Ryu et al. (2009) found that the GC hot plasma (*Plasma*) has two-temperature components, and hence the *Plasma* model can be described as

$$\text{Plasma} = \text{APEC1} + \text{APEC2} \text{ (photons s}^{-1} \text{ cm}^{-2}\text{)}, \quad (3)$$

where *APEC1* and *APEC2* are thin thermal plasma code in the XSPEC package for the low ( $kT_1$ ) and high ( $kT_2$ ) temperature components, respectively.

*Neutral* is composed of neutral lines and associated continuum emission, and hence can be given by

$$\text{Neutral} = \text{Abs2} \times [A \times (E/\text{keV})^{-\Gamma} + \text{Gaussians}] \text{ (photons s}^{-1} \text{ cm}^{-2}\text{)}, \quad (4)$$

where *Abs2* is self-absorption in the neutral clumps. Neutral lines are expressed by Gaussians, while the continuum is represented by a power-law model with the photon index  $\Gamma$  and the normalization *A*.

The cosmic X-ray background (CXB) flux is lower than the whole spectra shown in figure 2 by more than two orders of magnitude. We nevertheless add the CXB model made by Kushino et al. (2002),

$$\text{CXB} = \text{Abs1} \times \text{Abs1} \times 7.4 \times 10^{-7} \times (E/\text{keV})^{-1.41} \text{ (photons keV}^{-1} \text{ s}^{-1} \text{ cm}^{-2} \text{ arcmin}^{-2}\text{)}, \quad (5)$$

where absorption column density (*Abs1*) is applied twice because the origin of the CXB is extragalactic.

### 3.4. Spectral Fitting

Since the surface brightness of *Plasma* is not constant, the spectrum of *Neutral* cannot be directly obtained by the subtracting the surrounding (Reference) region. We therefore tried to simultaneous fit these two regions and to determine the spectra of the *Neutral* and *Plasma* models, separately.

The X-ray photons below  $\sim 2$  keV from the GC region are heavily absorbed by an inter-stellar medium of  $N_{\text{H}} \sim 6 \times 10^{22} \text{ cm}^{-2}$ , and the X-ray spectrum below  $\sim 2$  keV is dominated by the local background (Ryu et al. 2009). We therefore used only the 2–10 keV band for the spectral analysis.

In the fitting of *Plasma*, we assumed that the temperatures ( $kT_1$  and  $kT_2$ ) and elemental abundances (*Z*) of Si, S, Fe, and Ni were common in the two regions (Source and Reference). Abundances of Ar and Ca were set to be the same as that of S. Also, *Abs1* was treated to be common in the two regions. On the other hand, we set the normalizations of the hot plasma (*APEC1*, *APEC2*) to be independent free parameters.

For *Neutral*, common free parameters among the two regions are the power-law index ( $\Gamma$ ), the equivalent widths of the neutral lines to the continuum, and line center energies. The normalization of the power-law (*A*) is an independent free parameter. With these constraints, we proceeded the model fitting with equation (2) along the following 3 steps:

<sup>2</sup> [http://www.camdb.ac.cn/spectraspectra\\_search.asp](http://www.camdb.ac.cn/spectraspectra_search.asp)

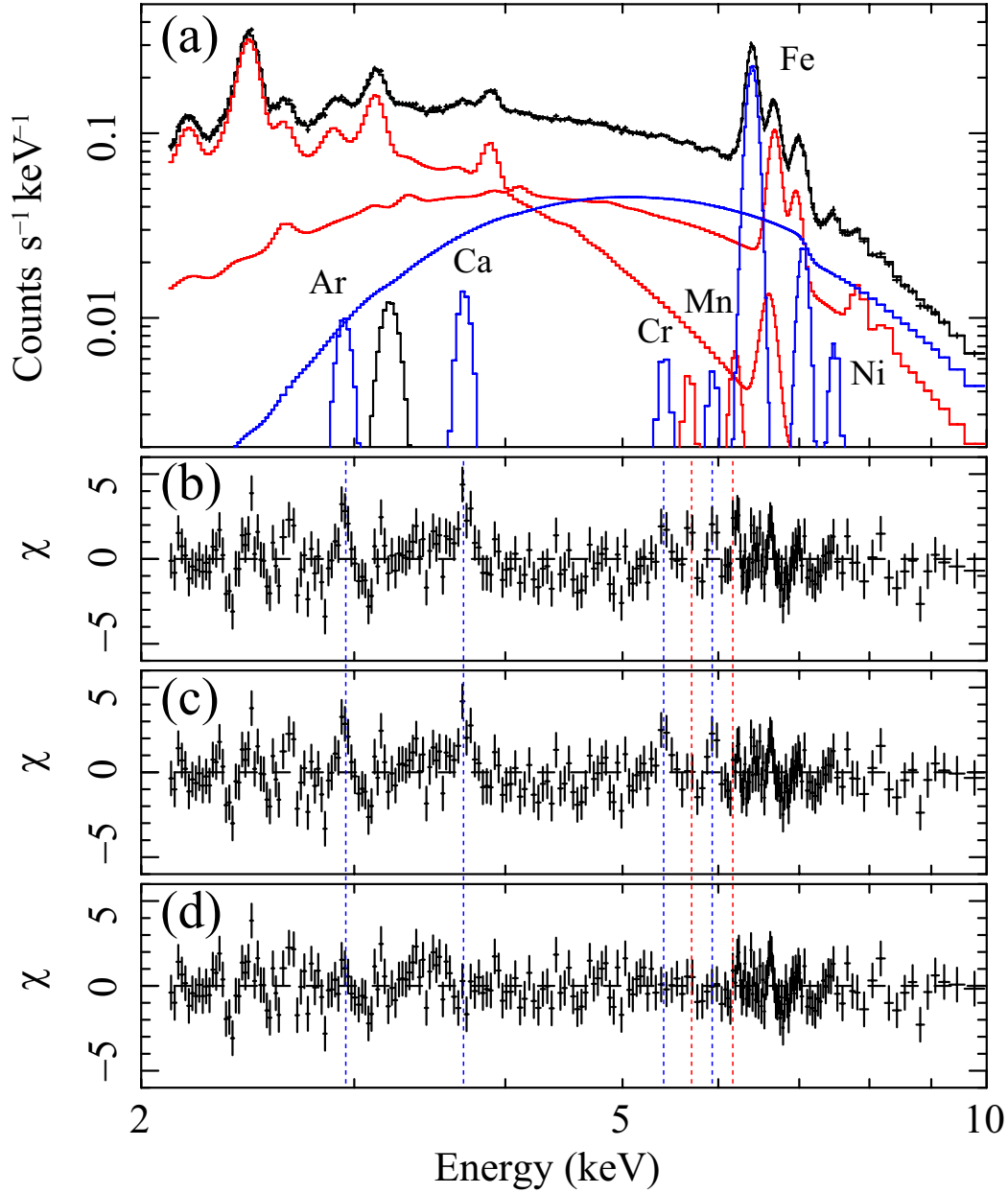


**Fig. 3.** (a): FI Spectrum of the Source region fitted with the final model (step 3) in subsection 3.4 (see text). The red and blue histograms are the best-fit *Plasma* and *Neutral* components, respectively. The Gaussian line at 3.2 keV is added to compensate the uncertainty of the instrumental response. The blue and red dashed lines indicate the energies of the neutral  $K\alpha$  of Ar, Ca, Cr, Mn and the He-like  $K\alpha$  of Cr and Mn. (b): Residual of the fitting with the models of 2- $kT$  *APEC*, a power-law, and neutral lines of Fe I  $K\alpha$ ,  $K\beta$ , Ni I  $K\alpha$  (step 1). (c): Same as (b), but the ionized Cr and Mn lines were added (step 2). (d): Same as (c), but the neutral Ar, Ca, Cr, and Mn  $K\alpha$  lines were added (step 3). Errors of the data were estimated at the  $1\sigma$  confidence level.

#### Step 1: Gaussians for K-shell Lines from Fe and Ni

For the *Neutral* model of equation 4, we first tried a fitting with three Gaussians for Fe I  $K\alpha$  (6.40 keV), Fe I  $K\beta$  (7.06 keV), and Ni I  $K\alpha$  (7.49 keV) lines (e.g. Koyama et al. 1996; Koyama et al. 2007b).

This fit left many residuals, including that at  $\sim 3.2$  keV. The energy is near the M-edge of Au (3.2–3.4 keV), and hence the residuals are likely due to the calibration uncertainty of the response of the XRT. In fact, similar residuals were reported by Kubota et al. (2007). We, thus,

added a broad Gaussian line at  $\sim 3.2$  keV according to Kubota et al. (2007). The best-fit center energy and the line width (1 sigma) of the Gaussian are  $3.24 \pm 0.02$  keV and  $0.07 \pm 0.02$  keV, respectively.

The fitting residuals are displayed simply for the FI spectra of the Source region in figure 3b, although the fitting was made simultaneously for the both sensors (FI and BI) and both the two regions. As shown in figure 3b, this model was not able to reproduce the observed spectra ( $\chi^2/\text{d.o.f}$  is 1447/906).



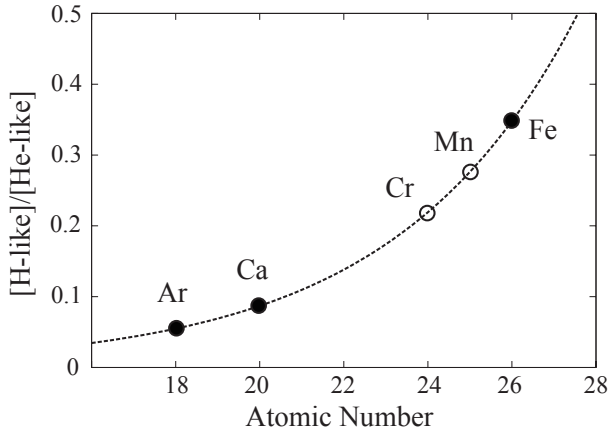


**Fig. 4.** Line-intensity ratios of He- and H-like ions. The filled circles are calculated values using the APEC model. The values of Ar, Ca, and Fe are 0.057, 0.085, and 0.35, respectively. By interpolating these data, the line intensity ratios of Cr and Mn are estimated to be 0.22 and 0.28 (open circles).

#### Step 2: K-shell Lines from Highly Ionized Cr and Mn

One reason of the unacceptable fit is that the APEC model does not contain Cr and Mn K-lines at 5–6 keV. We therefore added two Gaussian lines in the *Plasma* model of equation (3) at  $\sim 5.7$  and 6.2 keV for the Cr XXIII and Mn XXIV  $K\alpha$  lines, then, the center energies were obtained to be  $5.68 \pm 0.02$  and  $6.19 \pm 0.02$  keV, respectively. These are consistent with theoretical energies of 5.67 and 6.17 keV (CAMDB), the He-like Cr (Cr XXIII) and Mn (Mn XXIV).

The hot plasma can also emit  $K\alpha$  lines of H-like Cr (Cr XXIV) and Mn (Mn XXV) at 5.94 keV and 6.44 keV, respectively. Using the two-APEC model with the temperatures of 1 keV and 7 keV and the flux ratios given in table 2, we plotted the intensity ratio of H-like to He-like  $K\alpha$  lines as a function of atomic number (Ar, Ca, Fe) in figure 4. By interpolation, we estimated the line intensity ratios of Cr and Mn to be 0.22 and 0.28. We added these four lines in the *Plasma* model:

$$Plasma = APEC1 + APEC2 + 4Gaussians(Cr, Mn) \quad (\text{photons s}^{-1} \text{ cm}^{-2}), \quad (6)$$

where the intensity ratios of H-like to He-like Cr and Mn were fixed to be 0.22 and 0.28. We also set the equivalent widths of Cr XXIII  $K\alpha$  and Mn XXIV  $K\alpha$  to the continuum of the *Plasma* model to be the same in the two regions.

This fitting gave  $\chi^2/\text{d.o.f.}$  of 1367/902. The residuals from this model in the Source spectrum are shown in figure 3c. In the next step (step 3), we used the *Plasma* model of equation (6).

#### Step 3: K-shell Lines from Neutral Ar, Ca, Cr, and Mn

Since we still found line-like residuals at the energies of  $\sim 3.0$ , 3.7, 5.4, and 5.9 keV, we added four Gaussian lines to the *Neutral* model of equation (4) at these energies (in figure 3c, also see dashed lines in figure 3). Then

the line energies were found to be  $2.94 \pm 0.02$ ,  $3.69 \pm 0.02$ ,  $5.41 \pm 0.04$ , and  $5.94 \pm 0.03$  keV, respectively. These values correspond to theoretical energies of 2.96, 3.69, 5.41, and 5.90 keV for the  $K\alpha$  lines of Ar I, Ca I, Cr I, and Mn I. The fitting residuals in the spectrum of the Source region are shown in figure 3d.

As demonstrated in figure 3d, the  $\chi^2/\text{d.o.f.}$  is largely improved from 1367/902 (step 2) to 1203/894 (step 3), but is not acceptable even at the 99% confidence level. Although the energy resolution in the hard X-ray band is well calibrated with the calibration source  $^{55}\text{Fe}$  (emits the Mn I  $K\alpha$  line), that in the soft band, especially about 2 keV, may have some uncertainty due to the absence of available calibration sources. Thus the deviation at  $\sim 2.5$  keV would come from the incomplete response function in the soft energy band.

Residuals are also found at  $\sim 6.5$ –7.0 keV, with a slight mismatch of the center energy of Fe XXV  $K\alpha$ . This suggests that the GC hot plasma has more than two temperature components. We therefore tried a fitting with a three- $kT$  plasma model. Although the fit was improved from  $\chi^2/\text{d.o.f.}=1203/894$  to 1123/891, the best-fit parameters for the *Neutral* and *Plasma* models do not change from those in the two- $kT$  model within the statistical errors. We, thus, regard that the two- $kT$  model after step 3 is a good approximation to derive the physical parameters.

For the discussion on the neutral clump in the Source region, we list the best-fit parameters for the *Plasma* model in table 2, while those for the *Neutral* model are listed in table 3. For comparison, the best-fit parameters of the Reference region are: normalizations of *APEC1* and *APEC2* are  $6.8 \pm 0.5$  and  $0.90^{+0.06}_{-0.04}$  in the same unit shown in table 2, respectively. *Abs2* and normalization of the power-law component are  $12.7^{+1.2}_{-1.8} \times 10^{22} \text{ H cm}^{-2}$  and  $3.0^{+0.5}_{-0.4} \times 10^{-3} \text{ photons keV}^{-1} \text{ s}^{-1} \text{ cm}^{-2}$ , respectively. The other parameters are the same as the Source region.

## 4. Discussion

### 4.1. The GC hot plasma

The absorption column density toward the GC region (*Abs1*) is  $\sim 6.7 \times 10^{22} \text{ H cm}^{-2}$ , a typical value to the GC region (e.g., Munro et al. 2004). This is the first constrain that the low temperature  $kT = 1.01^{+0.01}_{-0.02} \text{ keV}$  plasma is also in the GC region.

Koyama et al. (2007b), using the same data set of this paper, reported the temperature of the GC hot plasma is  $kT = 6.5 \pm 0.1 \text{ keV}$ . The 1 keV plasma also emits Fe XXV  $K\alpha$ , but no significant Fe XXVI  $K\alpha$ . Since Koyama et al. (2007b) ignored the Fe lines from the 1.0 keV plasma, they under-estimated the flux ratio of Fe XXVI  $K\alpha$  to Fe XXV  $K\alpha$ , i.e., the plasma temperature. Indeed, about 20% of the Fe XXV  $K\alpha$  line may come from the 1.0 keV plasma. The flux ratio of the Fe lines is estimated to be 0.35 and 0.42 about the 6.5 keV and 7.0 keV plasmas by the APEC model, respectively. Taking the contribution of the low temperature plasma into account, the result in Koyama et al. (2007b) is consistent with our work.

The Fe and Ni abundances of 1.1–1.2 and 1.3–2.0 solar

**Table 3.** Fitting Results of *Neutral* and those of calculated values.\*

Neutral Lines					
Energy (keV)	Identification	Intensity <sup>†</sup>	EW(eV) <sup>‡</sup>	EW(XRN) <sup>§</sup>	EW(LECRE) <sup>§</sup>
$2.94 \pm 0.02$	Ar I K $\alpha$	$170^{+60}_{-40}$	$140 \pm 40$	45	12
$3.69 \pm 0.02$	Ca I K $\alpha$	$54^{+14}_{-9}$	$83 \pm 13$	35	10
$5.41 \pm 0.04$	Cr I K $\alpha$	$9.5 \pm 2.5$	$24 \pm 7$	10	3.5
$5.94 \pm 0.03$	Mn I K $\alpha$	$7.4 \pm 2.2$	$22 \pm 7$	7.6	2.8
$6.404 \pm 0.002$	Fe I K $\alpha$	$340 \pm 10$	$1150 \pm 90$	730	270
7.06 (fixed)	Fe I K $\beta$	$40 \pm 3$	$160 \pm 20$	120	38
$7.48 \pm 0.02$	Ni I K $\alpha$	$18 \pm 3$	$83 \pm 13$	53	18
Continuum					
Photon Index		$\Gamma$		$1.87 \pm 0.04$	
Normalization		$\parallel$		$9.6^{+1.6}_{-1.3}$	
$Abs2(N_H)$		$10^{22} \text{ cm}^{-2}$		$12.0 \pm 1.1$	

\*The uncertainties indicate the 90% confidence levels.

<sup>†</sup> Absorption-corrected line intensity in the unit of  $10^{-6} \text{ photon s}^{-1} \text{ cm}^{-2}$ .

<sup>‡</sup> Observed equivalent widths of the neutral lines to the power-law continuum in equation 4.

<sup>§</sup> Calculated equivalent widths in the XRN and LECE scenarios.

$\parallel$  Normalization at 1 keV in the unit of  $10^{-3} \text{ photons keV}^{-1} \text{ s}^{-1} \text{ cm}^{-2}$ .

**Table 2.** Fitting results of *Plasma*.\*

Component	Parameter	Unit	Value
<i>Abs1</i>	$N_H$	$10^{22} \text{ cm}^{-2}$	$6.75 \pm 0.13$
<i>APEC1</i>	$kT_1$	keV	$1.01^{+0.01}_{-0.02}$
	Norm	$\dagger$	$12 \pm 1$
<i>APEC2</i>	$kT_2$	keV	$7.0 \pm 0.1$
	Norm	$\dagger$	$1.3 \pm 0.1$
Abundances	Si	solar	$2.52^{+0.09}_{-0.17}$
	S, Ar, Ca	solar	$1.87 \pm 0.07$
	Fe	solar	$1.16^{+0.07}_{-0.04}$
	Ni	solar	$1.64 \pm 0.37$
Gaussian Lines			
Cr XXIII K $\alpha$	energy	(keV)	$5.68 \pm 0.02$
	EW	(eV)	$22 \pm 6$
Mn XXIV K $\alpha$	energy	(keV)	$6.19 \pm 0.02$
	EW	(eV)	$39 \pm 6$

\*The uncertainties indicate the 90% confidence levels.

<sup>†</sup> Emission measure  $10^{-12}/(4\pi D^2) \int n_e n_H dV$ , where  $D$  is the distance to the source (cm),  $n_e$  and  $n_H$  are the electron and hydrogen density ( $\text{cm}^{-3}$ ), respectively.

are more precise than the previous work (Koyama et al. 2007b). The abundances of lighter elements, Si and S, (Ar, Ca), were respectively determined to be 2.3–2.6 and 1.8–2.0 solar, for the first time. The highly ionized Cr and Mn lines in the GC region were discovered for the first time, but details are beyond the scope of this paper.

#### 4.2. Origin of the Neutral Clump

We discovered the K-shell lines of neutral Ar, Ca, Cr, and Mn from the bright neutral clump toward the Sgr A region at the significance levels of 6.8, 9.6, 6.1, and 5.4  $\sigma$ , respectively. The absorption column densities,  $N_H(Abs2)$  in the Source and Reference regions are  $12.0(\pm 1.1) \times 10^{22}$  and  $12.7^{+1.2}_{-1.8} \times 10^{22} \text{ cm}^{-2}$ , respectively.

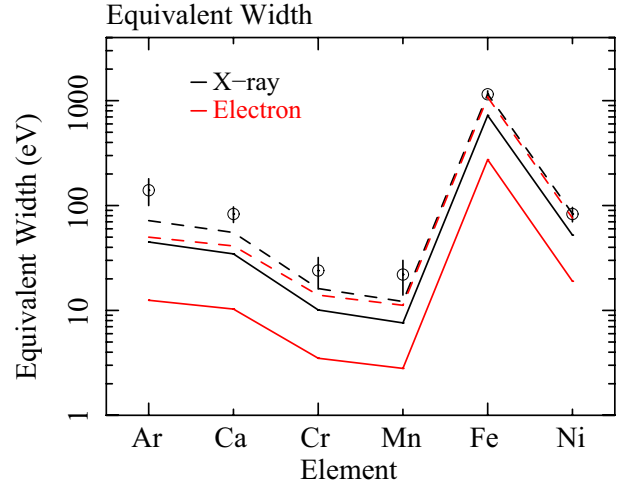


**Fig. 5.** Equivalent widths of K $\alpha$  line of various neutral atoms. Black and red lines are the calculated values for the X-ray (XRN) and electron (LECRE) scenarios, respectively. The data points marked with the open circles are the observed value in our work. Errors were estimated at the 90% confidence level. The black and red dashed lines are to guide eyes, which are XRN and LECRE scenarios in 1.6 solar and 4.0 solar abundances, respectively.

The photon index,  $\Gamma$  of the continuum (power-law) is  $1.87 \pm 0.04$ , which is consistent with the result of Koyama et al. (2009) in the same region. The equivalent widths of the neutral K $\alpha$  lines to the power-law continuum are  $\sim 140, 83, 24, 22, 1150, 83 \text{ eV}$  in Ar, Ca, Cr, Mn, Fe, and Ni, respectively.

The major possibility for the origin of the neutral clumps is the ionization of neutral atoms by either low energy cosmic-ray electrons (LECRE: Yusef-Zadeh et al. 2007) with an energy of 10–100 keV, or X-rays of external sources (XRN: Koyama et al. 1996; Murakami et al. 2000). The ionization cross-sections for these processes are very

different. They also produce a continuum emission: the bremsstrahlung in the LECRe scenario and Thomson scattering in the XRN scenario. As a result, the two scenarios make different X-ray spectra. In particular, sharp contrasts are the photon index of the continuum and the equivalent widths of the neutral lines.

The continuum emission in the X-ray spectrum produced by the LECRe scenario is an integration of the bremsstrahlung by electrons with various energies. According to Tatischeff (2003), we calculated the X-ray spectrum with various indexes of their energy distributions into a molecular cloud. As a result, the photon index of  $\Gamma = 1.9$  corresponds to an index of the LECRe source spectrum of  $\alpha \sim 3.0$ . On the other hand, the Thomson scattering do not change the photon index from the incident spectrum of the external source.

The equivalent width of the line is a good indicator for constraint of the origin. According to the calculation in Tatischeff (2003), the equivalent widths produced by the LECRe with the index  $\alpha = 3.0$  were estimated as shown with the red solid line in figure 5. Here, the elemental abundances in the neutral clump were assumed to be solar. On the other hand, Murakami et al. (2000) estimated the XRN spectrum by a numerical simulation. We improved the simulation (Murakami et al. 2000) to the other relevant elements. These are listed in table 3 and plotted in figure 5 together with the best-fit results.

From figure 5, the equivalent width of each element in the solar abundance is larger than that expected in the both of the LCREe and XRN scenarios. For the LCREe scenario, the abundances of the molecular cloud must be  $\sim 4$ -times larger than the solar value, while the XRN scenario requires  $\sim 1.6$  solar abundance.

Since the molecular cloud may be formed by condensation of the ambient materials, the abundances should be similar to those of 1–2 solar in the GC hot plasma. Accordingly, the neutral lines from the GC region likely come from the fluorescence by external X-rays. The photon index of  $\Gamma \sim 1.9$  is similar to the other neutral clumps in the Sgr B and C regions (Koyama et al. 2007c; Nobukawa et al. 2008; Nakajima et al. 2009), which suggests that the irradiating source is a single object, possibly a super-massive black hole, Sgr A\* (e.g., Murakami et al. 2000).

## 5. Summary

The summary of this work is as follows:

- We found that a  $kT = 1.0$  keV plasma exists in the GC region as well as the  $kT = 7.0$  keV plasma. The elemental abundances of Si, S (Ar, Ca), Fe, Ni were measured to be 2.3–2.6, 1.8–1.9, 1.1–1.2, 1.3–2.0 times larger than the solar value. We also discovered He-like Cr and Mn  $K\alpha$  lines from the GC region.
- K-shell lines of neutral Ar, Ca, Cr, and Mn were firstly discovered in addition to those of Fe and Ni. Equivalent widths of these atoms are  $\sim 140$ , 83, 24, 22, 1150, and 83 eV, respectively.

- The observed equivalent widths of Ar, Ca, Cr, Mn, Fe and Ni favor the X-ray radiation origin to the molecular cloud with 1–2 solar abundance.
- The power-law index of  $\Gamma = 1.9$  for the continuum emission is similar to the other neutral clumps, suggesting a single source origin, possibly the super-massive black hole Sgr A\*.

The authors thank H Matsumoto and H Uchiyama for their comments. This work is supported by the Grant-in-Aid for the Global COE Program "The Next Generation of Physics, Spun from Universality and Emergence" from the Ministry of Education, Culture, Sports, Science and Technology (MEXT) of Japan. This work is also supported by Grant-in-Aids from the Ministry of Education, Culture, Sports, Science and Technology (MEXT) of Japan, Scientific Research A, No. 18204015 (KK), and Scientific Research B, No. 20340043 (TT). MN is supported by JSPS Research Fellowship for Young Scientists.

## References

- Baganoff, F. K., et al. 2001, *Nature*, 413, 45  
 Baganoff, F. K., et al. 2003, *ApJ*, 591, 891  
 Fukuoka, R., Koyama, K., Ryu, S. G., & Tsuru, T. G. 2009, *PASJ*, 61, 593  
 Inui, T. et al. 2009, *PASJ*, 61, S241  
 Ishisaki, Y., et al. 2007, *PASJ*, 59, S113  
 Hyodo, Y., Ueda, Y., Yuasa, T., Maeda, Y., Makishima, K., & Koyama, K. 2009, *PASJ*, 61, S99  
 Koyama, K., Maeda, Y., Sonobe, T., Takeshima, T., Tanaka, Y., & Yamaichi, S. 1996, *PASJ*, 48, 249  
 Koyama, K., et al. 2007a, *PASJ*, 59, S23  
 Koyama, K., et al. 2007b, *PASJ*, 59, S245  
 Koyama, K., et al. 2007c, *PASJ*, 59, S221  
 Koyama, K., Takikawa, Y., Hyodo, Y., Inui, T., Nobukawa, M., Matsumoto, H., & Tsuru, G. T. 2009, *PASJ*, 61, S255  
 Kubota, A. et al. 2007, *PASJ*, 59, S185  
 Kushino, A., Ishisaki, Y., Morita, U., Yamasaki, N. Y., Ishida, M., Ohashi, T., & Ueda, Y., 2002, *PASJ*, 54, 327  
 Maeda, Y., et al. *ApJ*, 570, 671  
 Mitsuda, K., et al. 2007, *PASJ*, 59, S1  
 Munro, M. P., et al. 2004, *ApJ*, 613, 326  
 Murakami, H., Koyama, K., Sakano, M., Tsujimoto, M., & Maeda, Y. 2000, *ApJ*, 534, 283  
 Nakajima, H. et al. 2009, *PASJ*, 61, S233  
 Nobukawa, M. et al. 2008, *PASJ*, 60, S191  
 Ryu, G. S., Koyama, K., Nobukawa, M., Fukuoka, R., & Tsuru, G. T., 2009, *PASJ*, 61, 751  
 Serlemitsos, P., et al. 2007, *PASJ*, 59, S9  
 Tatischeff, V. 2003, in *Final Stage of Stellar Evolution*, ed. C. Motch & Hameury (EAS publication Series vol.7), 79 (astro-ph/0208397v1)  
 Tawa, N., et al. 2008, *PASJ*, 60, S11  
 Tsuboi, M., Handa, T., & Ukita, N. 1999, *ApJS*, 120, 1  
 Tsujimoto, M., Hyodo, Y., & Koyama, K. 2007, *PASJ*, 59, S229  
 Uchiyama, H., et al. 2009, *PASJ*, 61, S9  
 Yusef-Zadeh, F., Munro, M., Wardle, M., & Lis, D. C. 2007, *ApJ*, 656, 847